Geomechanics and Engineering, *Vol. 41, No. 3 (2025) 337-349*
https://doi.org/10.12989/gae.2025.41.3.337

Experimental research of polymer fracture under hydro-mechanical behavior

S.A. Reffas[1], M. Elmeguenni[1], M.S. Zagane[2], A. Moulgada[2], M. Yaylacı[*3,4,5], R. Yekhlef[6], Ş. Öztürk[3], M.E. Özdemir[7] and E. Uzun Yaylaci[8]

[1]*Department of Engineering Mechanics, University Djilali Liabes of sidi bel abbés, 22000, Algeria*
[2]*Department of Mechanical Engineering, University of Ibn Khaldoun Tiaret, 14000, Algeria*
[3]*Department of Civil Engineering, Recep Tayyip Erdogan University, 53100, Rize, Turkey*
[4]*Turgut Kıran Maritime Faculty, Recep Tayyip Erdogan University, 53900, Rize, Turkey*
[5]*Murat Yaylacı-Luzeri R&D Engineering Company, 53100, Rize, Turkey*
[6]*Research center in Industrial Technology, CRTI, P.O.Box 64 Cheraga, 16014, Algiers, Algeria*
[7]*Department of Civil Engineering, Cankiri Karatekin University, 18100, Çankırı, Turkey*
[8]*Faculty of Fisheries, Recep Tayyip Erdogan University, 53100, Rize, Turkey*

(*Received May 23, 2024, Revised March 31, 2025, Accepted April 2, 2025*)

Abstract. POM pipes are used to transport fluids. For this application, in-depth knowledge of the material's mechanical behavior and long-term performance is essential when subjected to mechanical stress. This article used an experimental approach based on macroscopic tests (thermal analysis technique for POM, tensile testing on notched axisymmetric specimens with measurement of the volume change), and complementary microscopic observations (MEB) to identify the cause of the damage**.** The results of the tests carried out at ambient temperature will be presented to show the influence of the type of control and the measurement principle (an assumption of homogeneous or isochoric deformation versus an assumption of transverse isotropic deformation) on the material's response.

Keywords: differential thermal analysis DTA; MEB; polyacetal; stress; thermogram DSC analysis; thermogravimetric

1. Introduction

Polyoxymethylene (POM) or Polyacetal stands out as a thermoplastic material that boasts a significant degree of crystallinity, which imparts it with high levels of strength and rigidity. Its inherent characteristics include excellent sliding properties, commendable wear resistance, and minimal moisture absorption. With commendable dimensional stability, fatigue resistance, and exceptional chemical resistance, POM emerges as a versatile construction material suitable for diverse applications. From producing intricate, small parts to meeting stringent surface quality standards, POM proves its mettle across various sectors. Moreover, the strength, rigidity, and dimensional stability of POM can be further enhanced by incorporating fillers such as organic, mineral, or glass variants, albeit at the cost of potential degradation in certain properties.

As can be understood from the mechanical advantages provided by POM, polymers are very reliable materials when used correctly, and there are interesting studies in the literature about their behavior in different cases. Che *et al.* (2022) reported that compressive strength increased strongly with increasing polymer content and specimen density. Polymer significantly affects mechanical strength, fracture behavior, and energy development. The fracture pattern of specimens with various polymer contents varies from single-path cracks to multi-path cracks. Tan *et al.* (2022) found a relationship between several mechanical properties of water-saturated sandstone and the pressures within the rock formation, specifically pore water pressure and confining pressure. Understanding these relationships can be essential for applications in geotechnical engineering, hydrology, and other fields related to subsurface engineering. Fazlollahi *et al.* (2019) presented a study of the hydro-mechanical drawing of sandwich sheets a complex topic involving integrating theoretical, numerical, and experimental analyses to understand and optimize the process. This type of drawing is critical in industries such as automotive and aerospace, where strong, lightweight structures are required. A safe region of fluid pressure was obtained to obtain a part without rupture. It is shown that the limit drawing rate increases with increasing the pressure, but after a certain, it decreases with increasing the chamber pressure. Cai *et al.* (2022) studied comprehensive hydrothermal aging on typical unidirectional flax fiber-reinforced phenolic resin composites (FFRP). This study spanned three years and included assessments at temperatures ranging from 23°C to 60°C. Throughout this period, the investigation focused on tracking changes in water uptake, microstructure, and mechanical properties of the FFRP to understand the aging mechanisms under hydrothermal conditions. Ouyang and Wang (2022) presented conducted under the NPT ensemble

*Corresponding author, Professor
E-mail: murat.yaylaci@erdogan.edu.tr

ISSN: 2005-307X (Print), 2092-6219 (Online)

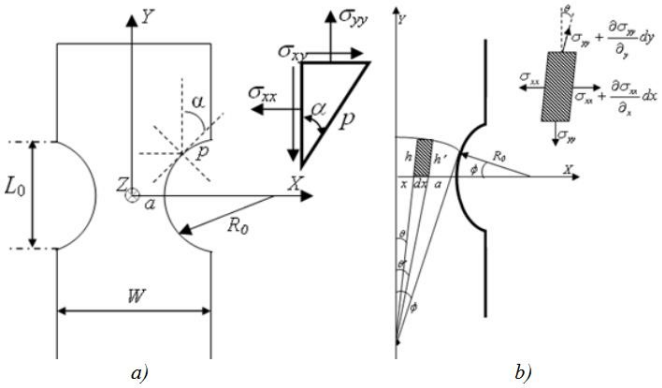

Fig. 1 Stress analysis schematic

at 4, 5.5, 8, and 12 MPa. The findings suggest that as pressure increases, there is a corresponding increase in the densification of the water-cellulose model. This impact on mechanical properties primarily stems from the extensive formation of hydrogen bonds within the cellulose chains and between the cellulose and water molecules. Tabasum *et al.* (2022) indicated that varying the cavity pressure significantly influences formability. Specifically, when the Variable Cavity Pressure (VCP) increased incrementally about punch strokes, the process achieved a maximum forming depth of 29.00 mm and yielded high-quality results. Conversely, progressively decreasing the VCP during forming led to less satisfactory outcomes. Ghadr *et al.* (2022) used to enhance soil quality typically increases soil strength and decreases cracking. A hydro-mechanical model has been created to forecast moisture movement and the beginning of desiccation cracks in unmodified and modified kaolin clays. The collected data revealed that the onset of desiccation cracks and radial displacements was postponed in the treated soil samples, corroborating the experimental observations. Özdemir and Yaylacı (2023) conducted a dynamic analysis of net cages made from various polymer materials in a fluid and compared the results. Milovanović *et al.* (2020) evaluated how various printing parameters affect the mechanical properties of standard PLA and PLA-X. An experimental setup involving variations in layer height, number of perimeters, infill density, and sample humidity was implemented. This comparison will help in understanding which material better suits specific applications and under which printing conditions. In addition to the studies summarized above that examine polymer materials in different cases, examining the studies investigating polymer-added materials (Jahangir *et al.* 2022, Frih *et al.* 2023, Ghatage *et al.* 2023, Kannan and Sujatha 2023, Swasdi *et al.* 2023, Wei *et al.* 2023, Yang and Mao 2023, Yazdani and Ashtiani 2023, Song *et al.* 2024) and those that solve problems with mathematical foundations will provide readers with a broader perspective (Al-Hdaibat *et al.* 2025a,b,c, Alqahtani *et al.* 2024, 2025, Khan *et al.* 2024).

The main objective of this work is to provide a comprehensive description of the mechanical properties of the study's base material, allowing for a better understanding of the deformation damage and fracture mechanisms of POM. Experimental studies conducted under different scenarios on POM pipes in the literature have not yet reached a level that can be verified numerically. This study will provide data that can be used to verify future studies. The authors base the novelty of this study on this fact. Following the presentation of the material under study, tests on flat specimens will be described. A significant part of this work involves setting up and carrying out mechanical tests on POM and discussing its mechanical behavior in large deformations. The results of the tests carried out at ambient temperature will be presented to show the influence of the type of control and the measurement principle (an assumption of homogeneous or isochoric deformation versus an assumption of transverse isotropic deformation) on the material's response.

2. Materials and methods

Researchers have always been interested in the mechanical behavior of complex materials under different boundary conditions (Turan *et al.* 2025, Aktarer *et al.* 2025, Abouelregal *et al.* 2025). Materials were examined using varius methods, some experimental (Bennedjadi *et al.* 2023, Chena *et al.* 2023, Guo *et al.* 2023) and some based on numerical analysis (Khaji and Fakoor 2022, Hua *et al.* 2023, Abdelmadjid *et al.* 2020, 2024, El Sallah *et al.* 2020, 2023, Sekban *et al.* 2024a,b,c, Selvamani *et al.* 2024a,b, 2025, Yaylacı *et al.* 2024a,b, 2025). Knowledge about the material's mechanical properties will greatly benefit during application. Polymers can provide physical advantages both in their base form and as additives. However, in addition to their mechanical analysis, attention should also be paid to their thermal analysis, as they can be thermally sensitive.

Many methods exist in the realm of thermal analysis techniques for polymers, each offering complementary insights that facilitate precise identification of material properties and transitions, along with their evolution over time.

2.1 Behavior on impact

Understanding the deformation and damage mechanisms requires exploring the material's mechanical response under various load conditions. Like other material classes, the

mechanical response of POM depends on the type of test, loading conditions, and the geometry of the specimens used.

Based on the analysis of the state of constraints during necking in a uniaxial tensile bar proposed by Bridgman (1944) and later adopted by Hill (1950), it is a flat specimen.

In the proposed assumption, the deformation analysis in the specimen's minimal section is assumed to be uniform. This assumption appears to be quite well validated on slightly notched specimens. However, the notching effect introduces additional stresses not all directed along the loading axis (uniaxial).

No exact solution provides the fields of constraints and deformations in a notched specimen. To properly define the stress distribution in a state of plane stress and in the vicinity of the notch, a schematic representation of the geometry of the test specimen is provided in Fig. 1(a), with a detailed stress distribution diagram in Fig. 1(b).

To analyze the tests on the evolution of the behavior of our polymer under a state of plane stress, we have considered the behavior of our material assumed to be perfectly elastic-plastic. This assumption is invalid for most polymer materials due to their large deformations. However, obtaining equilibrium equations for large deformations is very complex. In a Cartesian coordinate system, the mechanical equilibrium is then expressed as

$$\sigma_{ij} = 0 \tag{1}$$

When using flat test tubes with thin thicknesses, we assume that the stress distribution is planar, meaning that the stress representing the normal direction to the surface is considered zero and that the radial displacement in the minimum section is, proportional to the width. It is also inferred that the radial and circumferential deformations are equal and constant. Thus, the stress and strain tensors take the following form

$$\sigma = \begin{pmatrix} \sigma_{xx} & \sigma_{xy} & 0 \\ \sigma_{yx} & \sigma_{yy} & 0 \\ 0 & 0 & 0 \end{pmatrix} \tag{2}$$

and

$$\varepsilon = \begin{pmatrix} \varepsilon_{xx} & \varepsilon_{xy} & 0 \\ \varepsilon_{yx} & \varepsilon_{yy} & 0 \\ 0 & 0 & \varepsilon_{zz} \end{pmatrix} \tag{3}$$

This yields the following equilibrium equations

$$\begin{cases} \sigma_{xz} = \sigma_{yz} = 0 \\ \dfrac{\partial}{\partial z}[\ ] = 0 \\ \sigma_{zz} = 0 \end{cases} \tag{4}$$

Therefore, any point at the end of the notch depends only on two directions (x and y)

$$\begin{cases} \sigma_{xx} \cos\alpha = \sigma_{xy} \sin\alpha \\ \sigma_{yx} \cos\alpha = \sigma_{yy} \sin\alpha \end{cases} \tag{5}$$

In this case, the equations will be written as follows

$$\begin{cases} \sigma_{xx} = \sigma_{yy} \tan^2\alpha \\ \sigma_{yx} = \sigma_{yy} \tan\alpha \end{cases} \tag{6}$$

At the notch center Y = 0, where a = 0, we obtain

$$\begin{cases} \sigma_{xx}\big|_{x=0} = 0 \\ \sigma_{yx}\big|_{y=0} = 0 \end{cases} \tag{7}$$

$$\left.\frac{\partial \sigma_{yy}}{\partial y}\right|_{y=0} = 0 \tag{8}$$

The deformation along the Z-axis is given by the following formula

$$\varepsilon_{zz} = -\frac{1}{2}(\varepsilon_{xx} + \varepsilon_{zz}) \tag{9}$$

However, under these conditions of plane constraints, we assume that the constriction occurs after plasticization, and the following formula gives the equivalent stress used

$$\sigma_{eq} = \sqrt{\frac{1}{2}\left[(\sigma_{xx} - \sigma_{yy})^2 + (\sigma_{yy} - \sigma_{zz})^2 + (\sigma_{zz} - \sigma_{xx})^2\right]} \tag{10}$$

Where σ_{eq} represents the Von-Mises equivalent stress.

Based on these analyses, we can obtain straightforward solutions if the following conditions are met

$$\sigma_{yy} = \sigma_{xx} + \sigma_{yy}\big|_{y=a} = \sigma_{xx} + F \tag{11}$$

Or

$F = \sigma_{yy}\big|_{y=a}$ is the stress in the Y direction, satisfies the Von-Mises plasticity condition. This is a simplified equation where longitudinal effort is considered uniform across the entire section. However, finding another solution to solve the constraint equation in the transverse part of the constriction is possible by assuming that the contour forms a closed surface in the notch (Fig. 1(b)).

Based on Eq. (4), the main constraint line is perpendicular to the specimen's notch and center axes. It is reasonable to approximate by bringing the main constraints closer through a circle, with its center on the central axis (Fig. 1(a)).

Through a line perpendicular to the x-axis passing through point x, other lines can be constructed for the main constraints, assuming that these lines also form a circle and that these lines also construct the notch circle of the test specimen. For a very small angle f, the notch radius is considered R, and the circle radius is R', where R' = a/φ.

For a small section element with a unit width in the z-direction, bounded by x and x + dx, corresponding to the angle between the two axial lines θ and θ', the following equations can be obtained

$$\begin{cases} \theta = \dfrac{x\phi}{a} \\ \theta' = \dfrac{(x + dx)\phi}{a} = \dfrac{x\phi}{a} + \dfrac{dx\phi}{a} \end{cases} \tag{12}$$

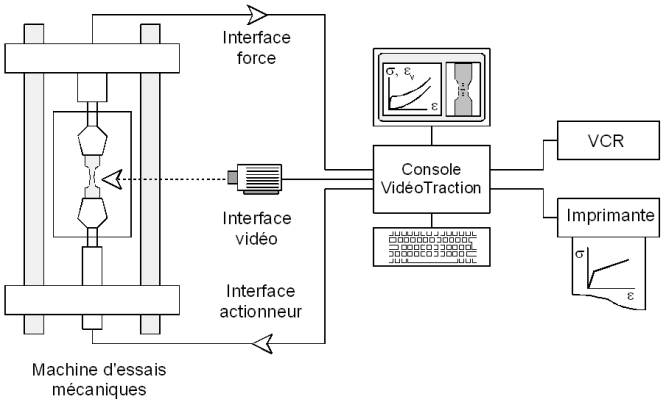

Fig. 2 INSTRON 5867 Press

Balancing efforts in the x-direction yields the following relationship

$$\left(\sigma_{yy}+\frac{\partial\sigma_{yy}}{\partial_y}dy\right)\sin\theta.dx-\sigma_{xx}h+\left(\sigma_{xx}+\frac{\partial\sigma_{xx}}{\partial x}dx\right)h'=0 \quad (13)$$

Based on the geometry of a flat specimen, the following relationship is obtained

$$\begin{cases} h=R\phi+R'(\cos\theta-\cos\phi) \\ h'=R\phi+R'(\cos\theta'-\cos\phi) \end{cases} \quad (14)$$

By substituting Eq. (12) into Eq. (14), with a small value of φ, and by introducing the following formula cosx=1-(x^2/2); we obtain the following equations

$$\begin{cases} h=\phi\left(R+\dfrac{a^2-x^2}{2a}\right) \\ h'=\phi\left(R+\dfrac{a^2-x^2}{2a}-\dfrac{x}{a}dx\right) \end{cases} \quad (15)$$

By substituting Eq. (15) into Eq. (13) with sin(x) = x, we obtain the following equations

$$\frac{d\sigma_{xx}}{dx}=-\frac{Fx}{a\left(R+\dfrac{a^2-x^2}{2a}\right)} \quad (16)$$

By integrating Eq. (16) into Eqs. (17) and (8), we ultimately obtain an approximate solution for the stress component σ_{xx}.

$$\sigma_{xx}=F\ln\left(\frac{a^2+2aR-x^2}{2aR}\right) \quad (17)$$

By adding Eq. (17) to Eq. (11) with the same boundary conditions as previously used, we ultimately obtain solutions for the other stress components.

$$\begin{cases} \sigma_{yy}=F\ln\left(1+\ln\left(\dfrac{a^2+2aR-x^2}{2aR}\right)\right) \\ \sigma_{zz}=0 \end{cases} \quad (18)$$

For a flat specimen with a groove of radius R_x at the bottom of a notch leaving, a remaining neck in the minimum section, the stress and strain distributions calculation is very complex and cannot be fully resolved analytically.

A tensile test involves subjecting a standardized specimen to a tensile force, typically until failure. Unless otherwise specified, the test is conducted at room temperature (20°C).

The strain measurement system relies on using a CCD video camera interfaced with a PC and mounted on a motorized stand, along with software enabling real-time image processing (Fig. 2). Video measurement allows for obtaining the deformations of materials under stress. It effectively replaces mechanical extensometers in most cases, particularly for large deformations and special environments. Its versatility enables adaptation to various specimen sizes and deformation paths. It directly provides stress-strain data for materials at imposed true strain rates. The method also allows for imposing a constant true radial strain rate and real-time measurement of the evolution of true axial stress.

However, this measurement technique allows for a more rational analysis of complex and varied experimental data.

The specimen, with a precisely defined geometry having average dimensions of 110 × 10 × 4 mm, is clamped at both ends into jaws or grips. One of these grips, fixed, is connected to a dynamometric system for force measurement using a ball joint so that the axis of the applied forces coincides with that of the specimen; the other grip, movable, is connected to a drive system at constant speed of displacement, or more rarely, constant load.

Dynamometric determinations (force measurements) are conducted using electronic sensors, typically consisting of a highly rigid elastic element (beam, ring, etc.), whose slight deformation due to the applied force is measured using an electrical system (strain gauges, variable inductances, capacitances, etc.).

In the case of a flat specimen (under plane stress), the local true axial strain and stress are given by the following relationships

$$\sigma_{yy}=\frac{F}{\left(S_0/\exp\left(\varepsilon_{zz}\right)\right)} \quad (19)$$

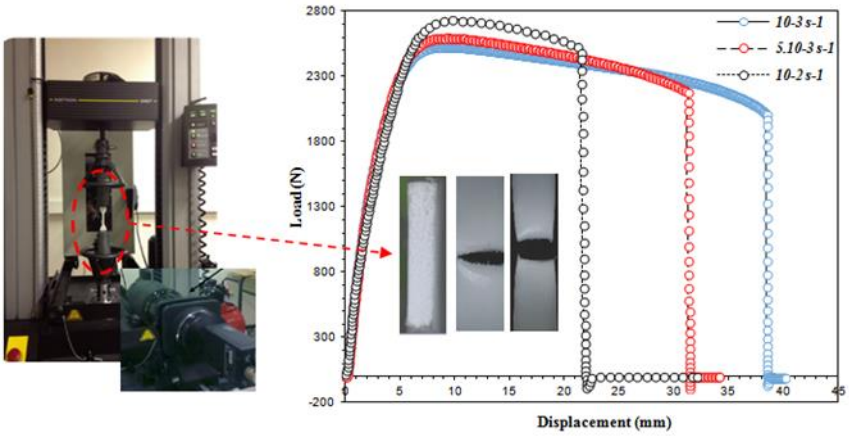

Fig. 3 Load-Displacement under different strain rates

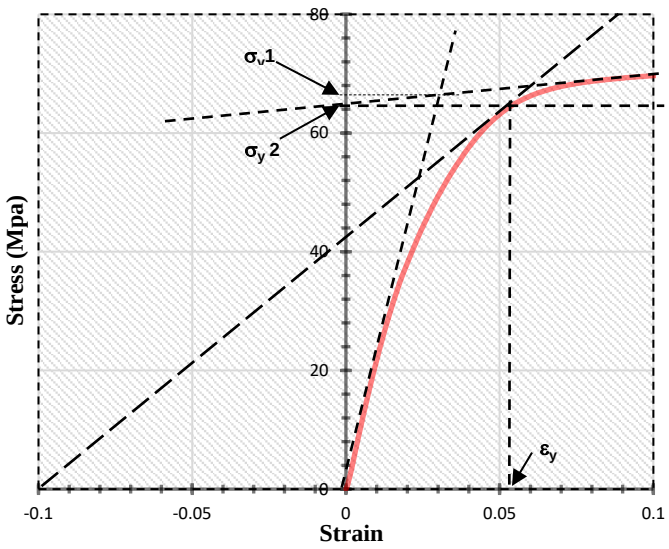

Fig. 4 Definitions of the plastic threshold

3. Results and discussion

The mechanical tests aim to characterize the law of material behavior. A behavior law establishes a relationship between stresses and strains. The tests are conducted controlled strain rates and at a temperature of 20°C. Large deformation tests were performed on an electromechanical machine of the Instron type (model 5867).

In Fig. 3, it is evident that for displacements ranging from 0 to 2, there is a correlation between the strain rate and the load observed at the plastic yield limit. Specifically, as the strain rate increases, the load at the plastic yield point also increases. However, beyond this point, a distinct softening phenomenon occurs, followed by a prolonged plateau phase, culminating in the initiation of hardening.

Young's modulus is determined in the linear segment of the stress-strain curve, where the stress is directly proportional to the strain. Furthermore, the end of this linear segment signifies the elastic limit, which appears before reaching the stress peak, denoted σ_y.

Performing tensile tests at different strain rates offers valuable insights into the behavior of polymers, shedding light on their intrinsic nature and response under different loading conditions.

Table 1 Mechanical properties of polyacetal

$d\varepsilon/dt$ (S^{-1})	E(MPa)	σ_y(MPa)	ν
0,0001	2143	63	0.38
0,0005	2254	66	
0,001	2325	70	

The yield stress and strain were determined graphically between the perfectly elastic region and the onset of plasticity of the true stress-strain curve (Fig. 4).

We thus see that when the deformation speed decreases, the initial plastic plateau is increasingly longer, and the hardening stage is delayed. The threshold stress was determined graphically between the perfectly elastic domain and the beginning of plasticity of the true stress-true strain curve (Fig. 4).

The mechanical properties of the polyacetal for the different speeds are given in Table 1.

The intersection of the origin tangent and the plateau tangent provides a value for the mechanical parameters.

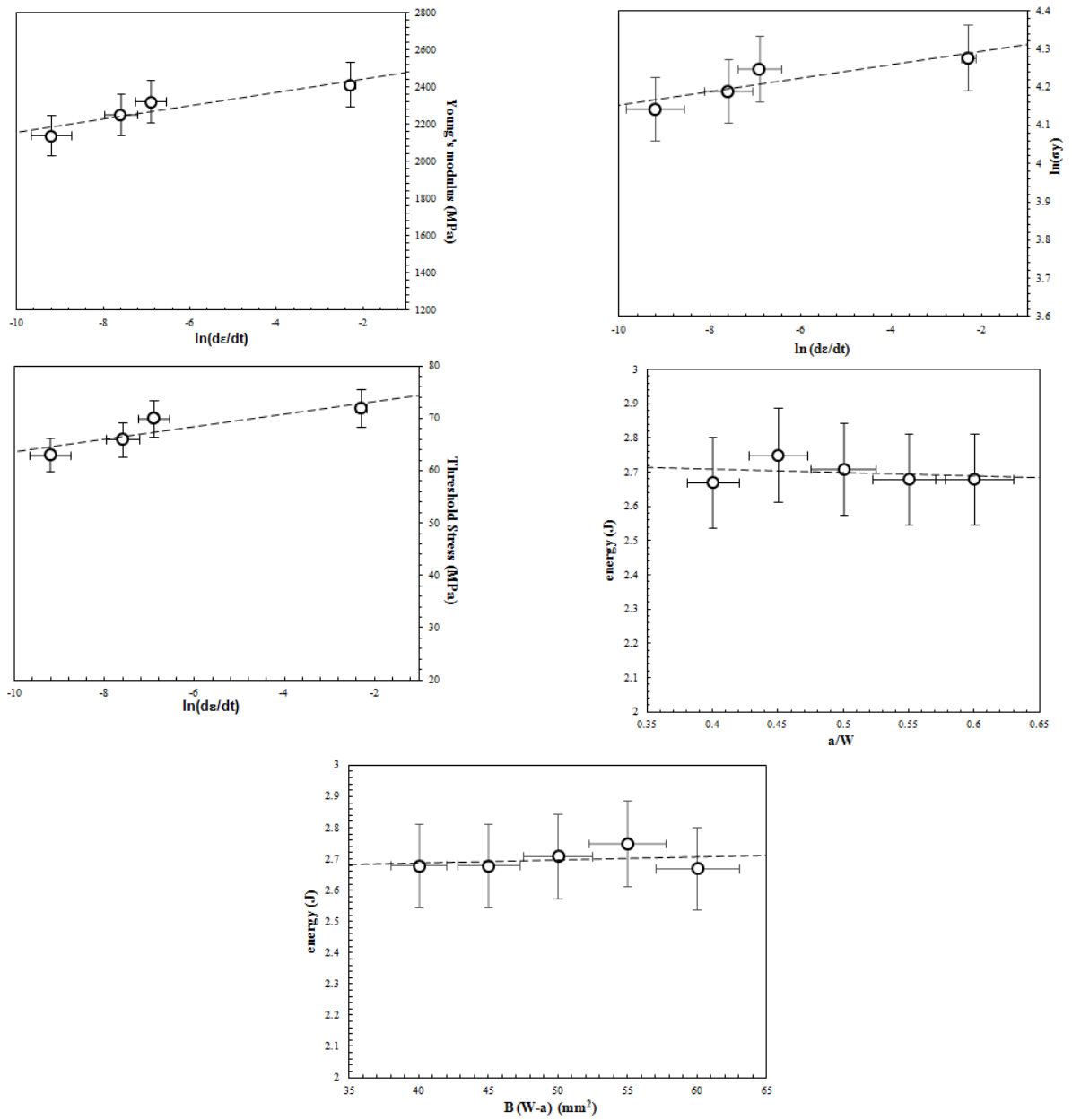

Fig. 5 Mechanical parameters relationship as a function of strain rate

Therefore, we propose to adopt this latter definition to determine the threshold plastic stress for all triaxialities. This evolution, as shown in Fig. 5, illustrates the dependence of POM threshold behavior on strain rate. In a first approximation, this evolution can be correlated by a linear regression with a relatively low slope.

Fig. 6 presents data on the variation of Young's modulus and POM energy on different samples.

The graph shows two sets of data: one for Young's modulus (a measure of the stiffness of a material) in percentage terms (E%) and another for energy in joules (J).

A black dotted line with data points indicates the trend in energy values, with error bars suggesting variability or uncertainty in the measurements. Similarly, Young's modulus also has error bars, although no connecting lines are drawn between these points.

The data shows that Young's modulus peaks at sample 2 and then decreases, while the measured energy shows a less clear trend but appears to decrease slightly after sample 2. This figure could suggest a correlation between Young's modulus and the energy characteristic of a new material or coating design, possibly indicating optimal properties for sample 2. The innovation may lie in how these two properties interact or are optimized in the new material design. This could imply that the material's stiffness (Young's modulus) directly affects its energy absorption or release characteristics (POM energy), which is important for applications where mechanical stiffness and energy management energy are crucial.

Fig. 7 shows a comparative analysis of impact strength and energy on five samples, presumably of one material, given the abbreviation POM commonly used for this thermoplastic.

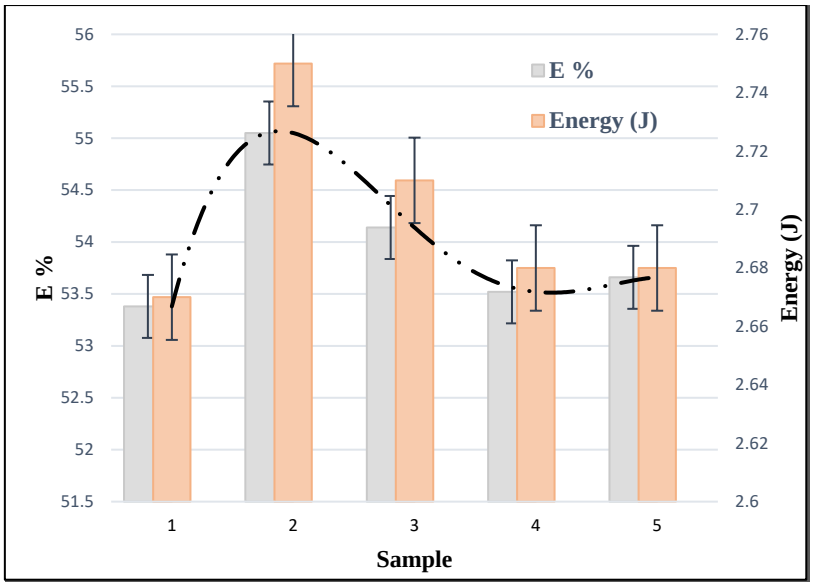

Fig. 6 The variation of young modulus and POM energy

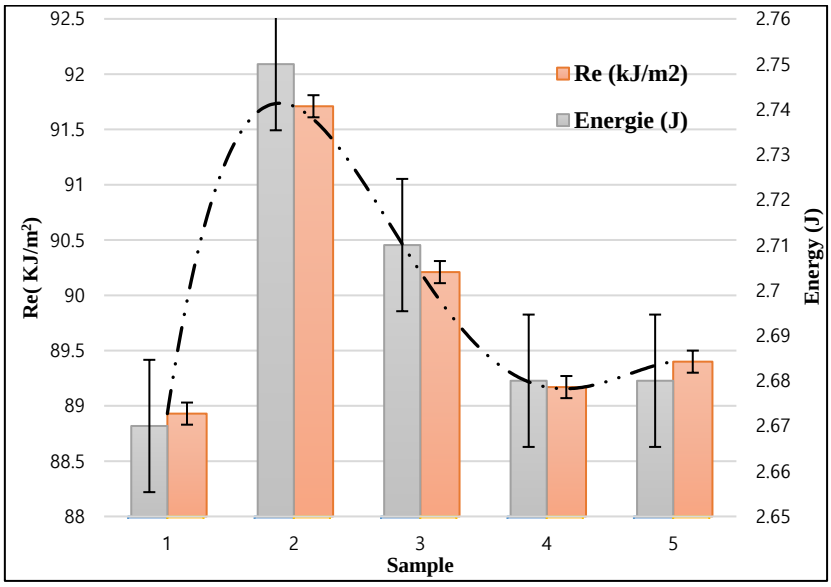

Fig. 7 The variation of impact strength and energy of POM

On the chart, there are two sets of data. A bar represents the impact resistance in kilojoules per square meter (Re (kJ/m²)), corresponding to the main y-axis on the left and the other mean energy in joules (Energy (J)), which relates to the secondary y-axis on the right – the variability or precision of measurements. Likewise, a dotted line connects the data points above the orange bars, again with error bars.

The graph shows that the impact strength peaks at sample 2 and then decreases. The energy also peaks at the sample 2 but experiences a less dramatic drop. There is a clear correlation between the trends in both properties, with sample 2 representing a peak in impact resistance and energy.

This figure can illustrate the mechanical properties of a new POM coating design. The focus would likely be on how the material's impact resistance correlates with its energy characteristics, which could be crucial for applications requiring materials that not only effectively absorb shock, but also effectively retain or dissipate impact energy. Innovation may lie in the formulation or processing of POM to improve these properties, with Sample 2 possibly representing an optimized balance between impact resistance and energy management. Such a balance could be critical to the material's function and purpose in practical applications, such as automotive parts, consumer electronics, or mechanical gears, where durability and impact resistance are essential.

In Fig. 8, micrographs of the fracture surface reveal the presence of voids, confirming the occurrence of structural damage. However, a noteworthy observation is the formation of damage bands consisting of numerous oriented and stretched voids. These bands exhibit an average size of

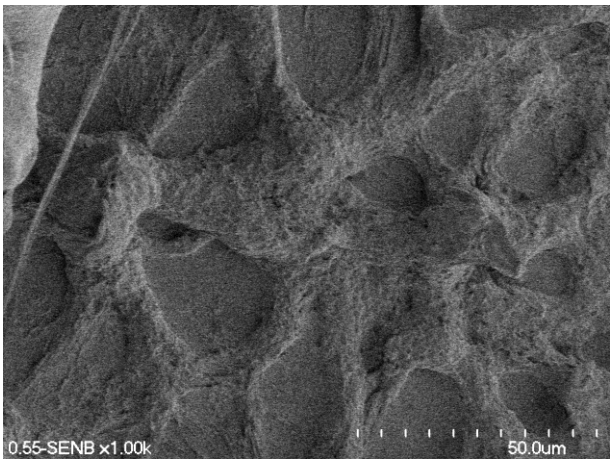

(a) 50 µm

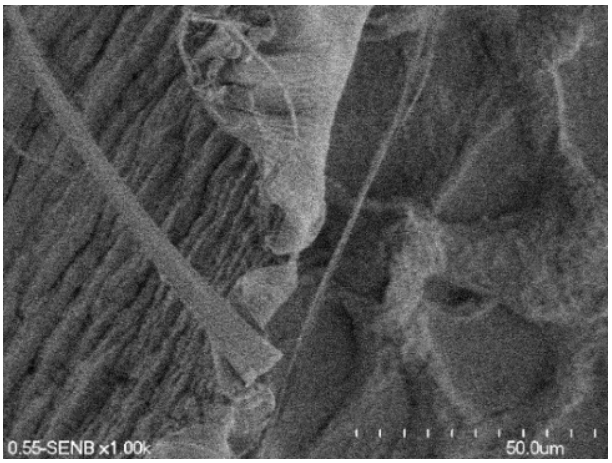

(b) 50 µm

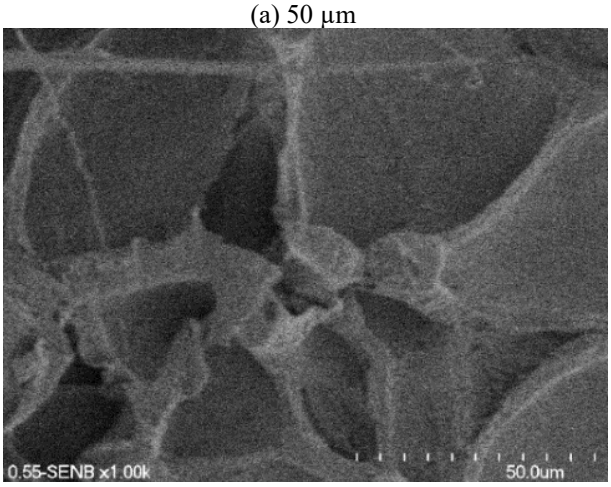

(c) 50 µm

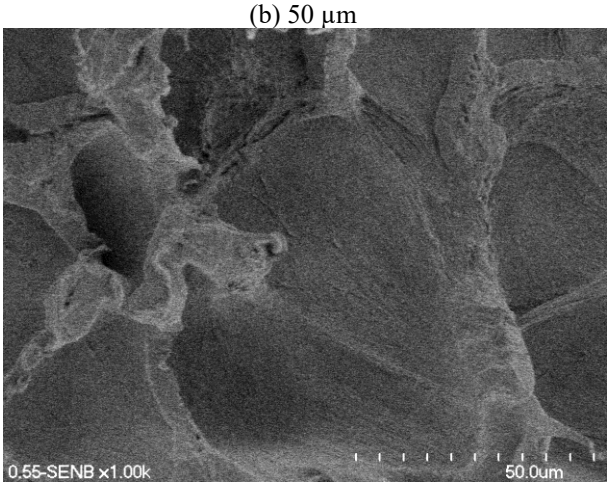

(d) 50 µm

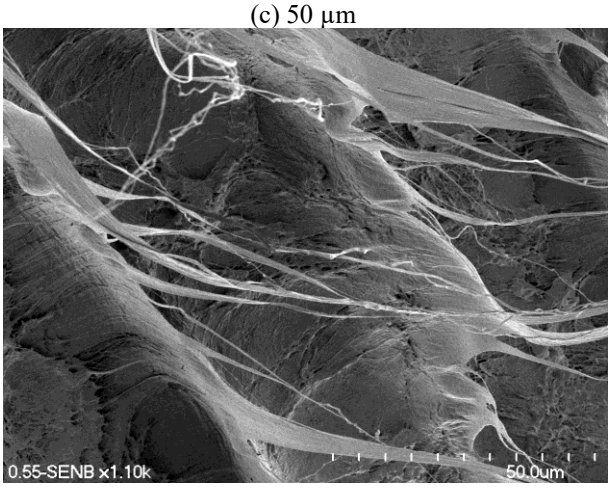

(e) 50 µm

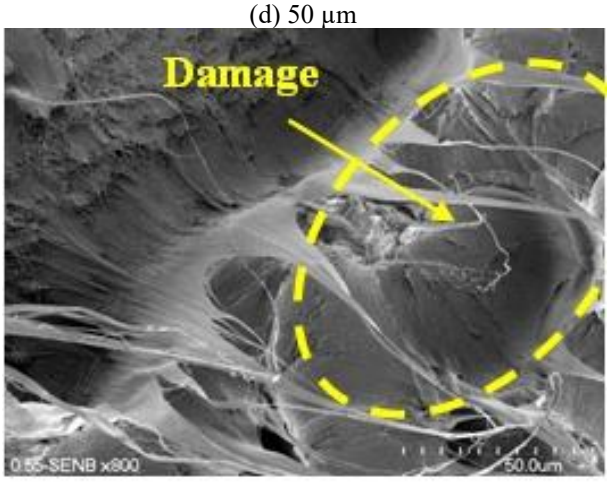

(f) 50 µm

Fig. 8 Observations (MEB) of the fracture surface: (a), (b), (c), (d) positions surrounding the initiation zone, (e) and (f) initiation zone

approximately 500 nm.

Upon comparing the micrographs, it becomes evident that the deformation mechanisms are markedly influenced by stress triaxiality. Specifically, significant cavitation fibrillation is observed under high triaxiality conditions, whereas at lower triaxiality, only a few diffuse voids are evident. This underscores the intricate relationship between stress conditions and the resulting deformation mechanisms, highlighting the importance of stress triaxiality in shaping material behavior and fracture characteristics.

Fig. 9 compares the monotonic response of POM in uniaxial tension at a strain rate of 10^{-1} s^{-1}. This figure highlights the loading path's influence on POM's behavior law. The behavior exhibits nearly zero hardening with a progressive stress drop after a strain greater than 5.5%.

During the thermo gravimetric analysis (ATG) presentation, it was elucidated that this technique serves as a powerful tool for characterizing both the physical and

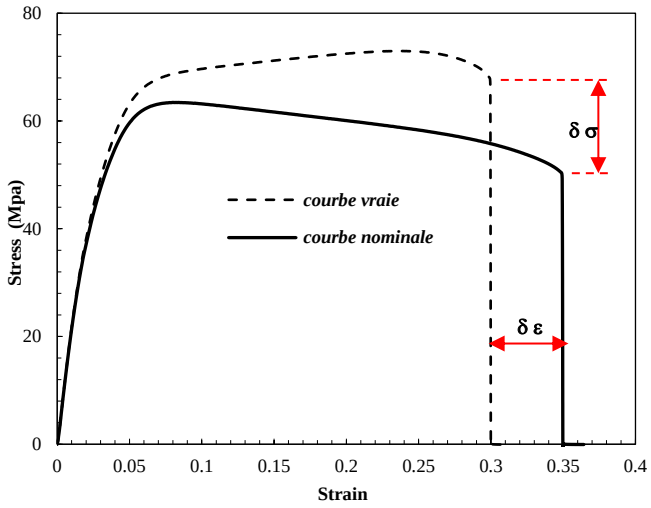

Fig. 9 Comparison between the results of the nominal and the true curve

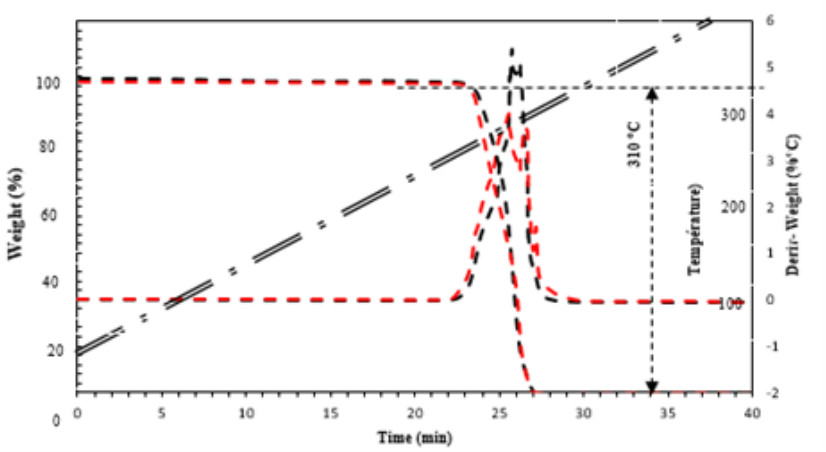

Fig. 10 Thermo gravimetric analysis

chemical properties of materials across a range of temperatures within a precisely controlled atmosphere. ATG enables researchers to observe changes in mass as a function of temperature, offering valuable insights into thermal stability, decomposition kinetics, and composition of materials.

Overall, thermo gravimetric analysis plays a pivotal role in the comprehensive characterization of materials, offering valuable information that aids in understanding their thermal behavior and chemical composition.

Differential scanning calorimetry (DSC) at a heating rate of 10 °C/min under nitrogen is used to evaluate the crystallinity ratio x_c of POM. The apparatus used is a Perkin-Elmer DSC Diamond, as shown on Fig. 10. The crystallinity ratio x_c is determined using the following relationship

$$x_c(\%) = \frac{\Delta H}{\Delta H_0} \times 100 \tag{21}$$

ΔH is the measured fusion enthalpy, and ΔH_0 is the theoretical fusion enthalpy of purely crystalline POM. The melting point T_m was also determined using DSC technique. This temperature corresponds to the maximum value of the peak. The thermographs corresponding to the three positions are shown on Fig. 11.

The crystallinity ratio of POM is around 40%.

During the DSC analysis presentation, we saw that this method can provide values such as the melting temperature, the crystallization temperature, and the crystallization rate.

The AMD analysis allowed us to obtain the following values: the storage modulus in tension (E'), the corresponding loss modulus (E″), and the mechanical loss angle tan δ.

The storage modulus E' (Fig. 12) stands for the stiffness and elastic component of the material. It refers to the body's ability to store mechanical energy from stress and fully recover it in the form of elastic deformation (the notion of reversibility), and the loss modulus E" represents the viscous component of the material. Viscosity reflects the capability to distribute mechanical energy (irreversibly lost as heat). This phenomenon is related to the friction and flow of molecular chains.

The mechanical dissipation angle (or damping factor) tan δ is a measure of the ratio of the energy dissipated by damping to the elastic energy stored and subsequently

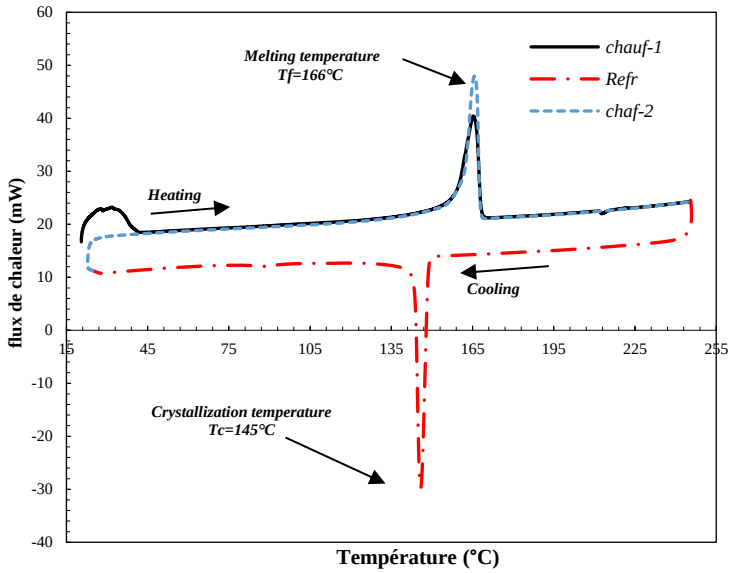

Fig. 11 DSC thermogram of POM

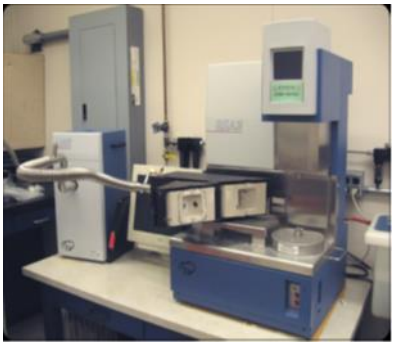

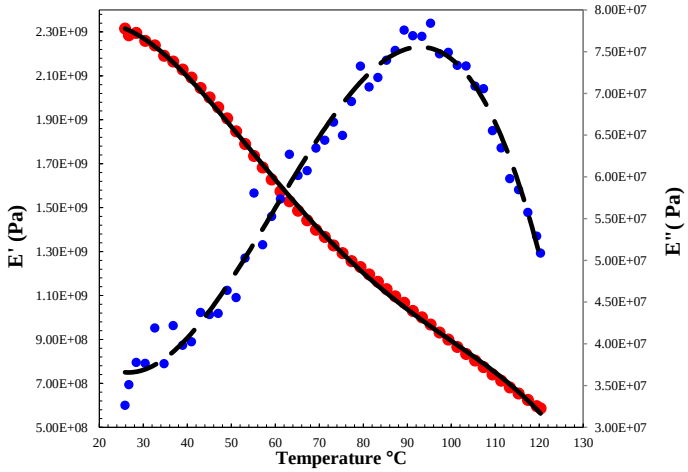

Fig. 12 Balance of storage modulus (E') and loss modulus (E'')

restored during a sinusoidal deformation cycle (Fig. 13). It measures damping during dynamic deformation and indicates the ability of the viscoelastic body to dissipate mechanical energy as heat. The higher the phase angle, the greater the vibration damping.

These curves once again reveal that POM has unique properties, making it challenging to find a material that can replace it.

4. Conclusions

As anticipated from the outset, substituting POM proves to be a formidable challenge due to its distinct and unparalleled properties. Finding an equivalent material that matches its specific characteristics is no small feat.

In conclusion, we have successfully achieved the primary objective of this study, which was to provide a comprehensive description of the mechanical, physical, and thermal properties of POM, along with identifying potential alternative polymers. However, finding a perfect replacement for POM remains elusive.

Moving forward, to effectively model the behavior exhibited by POM, it becomes imperative to develop a plastic law that accounts for damage mechanisms, particularly focusing on void growth and coalescence, even under extremely large deformations. This will be crucial for accurately simulating and predicting the behavior of materials exhibiting similar properties to POM.

References

Abdelmadjid, M., El Sallah, Z.M., Abderahmane, S., kaciDjafar, A. and Rachid, Z. (2020), "Comparative study of the repair of cracked plates with two different composite patches", *Frattura ed Integrità Strutturale*, **14**(53), 187-201.

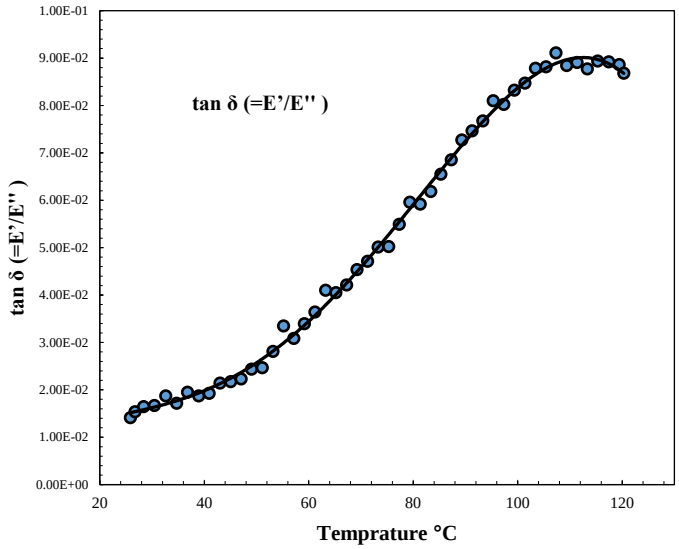

Fig. 13 Balance of mechanical loss angle tan δ

https://doi.org/10.3221/IGF-ESIS.53.16.

Abdelmadjid, M., El Sallah, Z.M., Yaylacı, M., Djafar, A.K., Ali, B., Abdelghani, B. and Uzun Yaylacı, E. (2024), "Effects of the stiffness of an inclusion on the mechanical behavior of an aluminum alloy plate with a lateral notch", *Steel Compos. Struct.,* **51**(1), 63-72. https://doi.org/10.12989/scs.2024.51.1.063.

Abouelregal, A.E., Alsaeed, S.S., Yaylacı, M., Elzayady, M.E., Kurt, Z. and Uzun Yaylacı, E. (2025), "The dual phase lag model for thermoelastic microbeams embedded in an elastic foundation incorporating fractional Kelvin–Voigt viscoelasticity", *Mech. Mater.*, 105336. https://doi.org/10.1016/j.mechmat.2025.105336.

Aktarer, S.M., Kucukomeroglu, T., Sekban, D.M., Uzun Yaylacı, E., Yaylacı, M., Özdemir, M.E. and Mirzaloglu, İ. (2025), "Analysis of the changes in microstructure, mechanical, and contact properties of multi-pass friction stir processed DP800 steel", *Adv. Nano Res.*, **18**(3), 253-264. https://doi.org/10.12989/anr.2025.18.3.253.

Al-Hdaibat, B., DarAssi, M.H., Ahmad, I., Khan, M.A., Algethamie, R. and Alzahrani, E. (2025a), "Numerical investigation of an SIR fractional order delay epidemic model in the framework of Mittag–Leffler kernel", *Nonlinear Dyn.*, **113**, 17289-17309. https://doi.org/10.1007/s11071-025-11006-5.

Al-Hdaibat, B., DarAssi, M.H., Ahmad, I., Altaf Khan, M. and Algethamie, R. (2025b), "Investigating tuberculosis dynamics under various control strategies: A comprehensive analysis using real statistical data", *Math. Meth. Appl. Sci.*, https://doi.org/10.1002/mma.10779.

Al-Hdaibat, B., Sabra, R., DarAssi, M.H. and Al-Ashhab, S. (2025c), "On the Recursive Sequence xn+ 1= axn− 1 b+ cxnxn− 1", *Mathematics*, **13**(5), 823. https://doi.org/10.3390/math13050823.

Alqahtani, Z., Almuneef, A., DarAssi, M.H., AbuHour, Y., Al-arydah, M.T., Safi, M.A. and Al-Hdaibat, B. (2024), "Mathematical analysis of fractional Chlamydia pandemic model", *Sci. Rep.*, **14**, 31113. https://doi.org/10.1038/s41598-024-82428-1.

Alqahtani, Z., DarAssi, M.H., AbuHour, Y. and Almuneef, A. (2025), "Assessing the role of vaccination in the control of hand, foot, and mouth disease transmission", *Mathematics*, **13**(2), 268. https://doi.org/10.3390/math13020268.

Bennedjadi, M., Aldosari, S.M., Chikh, A., Kaci, A., Bousahla, A. A., Bourada, F. and Tounsi, A. (2023), "Visco-elastic foundation effect on buckling response of exponentially graded sandwich plates under various boundary conditions", *Geomech. Eng.*, **32**(2), 159-177. https://doi.org/10.12989/gae.2023.32.2.159.

Bridgman, P.W. (1944), "The stress distribution at the neck of a tension specimen", *Trans. ASM*, **32**, 553-574.

Cai, M., Zhang, X., Sun, B., Takagi, H., Waterhouse, G.I. and Li, Y. (2022), "Durable mechanical properties of unidirectional flax fiber/phenolic composites under hydrothermal aging", *Compos. Sci. Technol.*, **220**, 109264. https://doi.org/10.1016/j.compscitech.2022.109264.

Che, W., Liu, J., Li, H., He, C., Bai, Y., Song, Z., Wang, Y., Qian, W. and Chen, Z. (2022), "Experimental investigation and discrete element method simulation on mechanical properties and failure mechanism of polymer-stabilized sand", *Bull. Eng. Geol. Environ*., **81**, 1-22. https://doi.org/10.1007/s10064-021-02516-8.

Chena, S., Visintin, P. and Oehlers, D.J. (2023), "Experimental investigation of the influence of fibre content on the flexural performance of simply supported and continuous steel/UHPC composite slabs", *Steel Compos. Struct.*, **49**(5), 571-858. https://doi.org/10.12989/scs.2023.49.5.571.

El Sallah, Z.M., Abdelmadjid, M., Abderahmane, S., Abdelghani, B. and Ali, B. (2023), "Study of the fracture behavior of different structures by the extended finite element method (X-FEM)", *Adv. Mater. Res*., **12**(4), 273-286. https://doi.org/10.12989/amr.2023.12.4.273.

El Sallah, Z.M., Benouis, A., Moulgada, A., Djebbar, N. and Sahli, A. (2020), "Biomechanical behaviour of the total hip prosthesis subjected to normal gait cycle load: Identification of the damage in the cement mantle", *J. Serb. Soc. Comput. Mech.*, **14**(2), 14-30.

Fazlollahi, M., Morovvati, M.R. and Mollaei Dariani, B. (2019), "Theoretical, numerical and experimental investigation of hydro-mechanical deep drawing of steel/polymer/steel sandwich sheets", *Proc. Inst. Mech. Eng. Pt. B J. Eng. Manufact.*, **233**(5), 1529-1546. https://doi.org/10.1177/0954405418780173.

Frih, A., Bourada, F., Kaci, A., Bouremana, M., Tounsi, A., Al-Osta, M.A. and Salem, M. A. (2023), "A novel hyperbolic integral-Quasi-3D theory for flexural response of laminated composite plates", *Geomech. Eng.*, **34**(3), 233-250. https://doi.org/10.12989/gae.2023.34.3.233.

Ghadr, S., Liu, C.H., Mrudunayani, P. and Hung, C. (2022), "Effects of hydrophilic and hydrophobic nanosilica on the hydromechanical behaviors of mudstone soil", *Constr. Build. Mater*., **331**, 127263. https://doi.org/10.1016/j.conbuildmat.2022.127263.

Ghatage, P.S., Sudhagar, P.E. and Kar, V.R. (2023), "Free vibrational behavior of perfect and imperfect multi-directional FG plates and curved structures", *Geomech. Eng.*, **35**(4), 367-383. https://doi.org/10.12989/gae.2023.35.4.367.

Guo, Y., Zhang, Q., Wang, H., Liu, R., Chen, X., Li, W. and Zhang, L. (2023), "Experimental study of strength characteristics of reinforced broken rock mass", *Geomech. Eng.*, **33**(6), 553-565. https://doi.org/10.12989/gae.2023.33.6.553.

Hill, R. (1950), "The mathematical theory of plasticity" Clarendon Press, Oxford.

Hua, S., Shokravi, M. and Wang, S.S. (2023), "Mathematical model for rock-soil slope stability based on numerical solution", *Geomech. Eng.*, **35**(3), 307-313. https://doi.org/10.12989/gae.2023.35.3.307.

Jahangir, H., Eidgahee, D.R. and Esfahani, M.R. (2022), "Bond strength characterization and estimation of steel fibre reinforced polymer-concrete composites", *Steel Compos. Struct.*, **44**(6), 803-816. https://doi.org/10.12989/scs.2022.44.6.803.

Kannan, G. and Sujatha, E.R. (2023), "A study on the efficacy of low viscous nanosized biopolymer on the mechanical and hydraulic properties of organic silt", *Geomech. Eng.*, **34**(3), 221-231. https://doi.org/10.12989/gae.2023.34.3.221.

Khaji, Z. and Fakoor, M. (2022), "Enhancing the ability of strain energy release rate criterion for fracture assessment of orthotropic materials under mixed-mode I/II loading considering the effect of crack tip damage zone", *Steel Compos. Struct.*, **44**(6), 817-828. https://doi.org/10.12989/scs.2022.44.6.817.

Khan, M.A., DarAssi, M.H., Ahmad, I., Seyam, N.M and Alzahrani, E. (2024), "Modeling the dynamics of tuberculosis with vaccination, treatment, and environmental impact: fractional order modeling", *Comput. Model. Eng. Sci*., **141**(2), 1365-1394. https://doi.org/10.32604/cmes.2024.053681.

Milovanović, A., Sedmak, A., Grbović, A., Golubović, Z., Mladenović, G., Čolić, K. and Milošević, M. (2020), "Comparative analysis of printing parameters effect on mechanical properties of natural PLA and advanced PLA-X material", *Procedia Struct. Integr*., **28**, 1963-1968. https://doi.org/10.1016/j.prostr.2020.11.019.

Ouyang, F. and Wang, W. (2022), "Effect of thermo-hydro-mechanical treatment on mechanical properties of wood cellulose: A molecular dynamics simulation", *Forests*, **13**(6), 903. https://doi.org/10.3390/f13060903.

Özdemir, M.E. and Yaylacı, M. (2023), "Research of the impact of material and flow properties on fluid-structure interaction in cage systems", *Wind Struct.*, **36**(1), 31-40. https://doi.org/10.12989/was.2023.36.1.031.

Sekban, D.M., Uzun Yaylacı, E., Özdemir, M.E. and Yaylacı, M. (2024a), "Determination of formability behavior of steel used in ships by various methods", *Struct. Eng. Mech.*, **92**(2), 189-196. https://doi.org/10.12989/sem.2024.92.2.189.

Sekban, D.M., Uzun Yaylacı, E., Özdemir, M.E., Öztürk, Ş., Yaylacı, M. and Panda, S.K. (2024b), "Formability behavior of AH-32 shipbuilding steel strengthened by friction stir process", *Theor. Appl. Fract. Mech.*, **132**, 104485. https://doi.org/10.1016/j.tafmec.2024.104485.

Sekban, D.M., Uzun Yaylacı, E., Özdemir, M.E., Yaylacı, M. and Tounsi, A. (2024c), "Investigating formability behavior of friction stir-welded high-strength shipbuilding steel using experimental, finite element, and artificial neural network methods", *J. Mater. Eng. Perform*., 1-9. https://doi.org/10.1007/s11665-024-09501-8.

Selvamani, R., Loganathan, R., Yaylacı, M., Uzun Yaylacı, E. and Özdemir, M.E. (2024b), "Vibration of piezo-magneto-thermoelastic FG nanobeam submerged in fluid with variable nonlocal parameter", *Adv. Nano Res.,* **16**(5), 489-500. https://doi.org/10.12989/anr.2024.16.5.489.

Selvamani, R., Prabhakaran, T., Yaylacı, M., Kartal, Ş.E. and Uzun Yaylacı, E. (2025), "Doublet structural modeling of nonhomogeneous Euler mass sensor nanobeams using boundary characteristics Bernstein Polynomials", *ZAMM Z. fur Angew. Math. Mech.*, **105**(3), e202401264. https://doi.org/10.1002/zamm.202401264.

Selvamani, R., Thangamuni, P., Yaylacı, M., Emin Özdemir, M. and Uzun Yaylacı, E. (2024a), "Nonlinear vibration and parametric excitation of magneto-thermo elastic embedded nanobeam using homotopy perturbation technique", *ZAMM Z. fur Angew. Math. Mech.*, **104**(12), e202400525. https://doi.org/10.1002/zamm.202400525.

Song, J.P., She, G.L. and He, Y.J. (2024), "Nonlinear forced vibration of axially moving functionally graded cylindrical shells under hygro-thermal loads", *Geomech. Eng.*, **36**(2), 99-109. https://doi.org/10.12989/gae.2024.36.2.099.

Swasdi, S., Iyaruk, A., Promputtangkoon, P. and Lukjan, A. (2023), "Compressive and tensile strength behaviors of sand reinforced with fibers and natural Para rubber", *Geomech. Eng.*, **32**(4), 561-573. https://doi.org/10.12989/gae.2023.32.4.361.

Tabasum, M.N., Lang, L., Mirza, H.A., Meng, Z. and Blala, H. (2022), "Numerical and experimental investigations on the effects of variable cavity pressure on the formability of GLARE using hydromechanical deep drawing", *J. Adv. Manuf. Technol*., **119**(9), 6091-6101. https://doi.org/10.1007/s00170-021-08518-w.

Tan, T., Zhao, Y., Zhao, X., Chang, L. and Ren, S. (2022), "Mechanical properties of sandstone under hydro-mechanical coupling", *Appl. Rheology*, **32**(1), 8-21. https://doi.org/10.1515/arh-2022-0120.

Turan, M., Kahya, V., Uzun Yaylacı, E. and Yaylacı, M. (2025), "A shear deformable numerical approaches for the static analysis of bi-directional functionally graded beams", *Adv. Nano Res.*, **18**(2), 143-162. https://doi.org/10.12989/anr.2025.18.2.143.

Wei, C., Shao, Y., Hassanein, M. F., Xiong, C. and Zhu, H. (2023), "Static strengths of preloaded circular hollow section stub columns strengthened with carbon fiber reinforced polymer", *Steel Compos. Struct.*, **47**(4), 455-466. https://doi.org/10.12989/scs.2023.47.4.455.

Yang, Y. and Mao, Y. (2023), "Effect of cross-section geometry on the stability performance of functionally graded cylindrical imperfect composite structures used in stadium construction", *Geomech. Eng.*, **35**(2), 181-194. https://doi.org/10.12989/gae.2023.35.2.181.

Yaylacı, M., Uzun Yaylacı, E., Turan, M., Özdemir, M.E., Öztürk, Ş. and Ay, S. (2024a), "Research of the crack problem of a functionally graded layer", *Steel Compos. Struct.,* **50**(1), 77-87. https://doi.org/10.12989/scs.2024.50.1.077.

Yaylacı, M., Yaylı, M., Öztürk, Ş., Ay, S., Özdemir, M.E., Uzun Yaylacı, E. and Birinci, A. (2024b), "Examining the contact problem of a functionally graded layer supported by an elastic half-plane with the analytical and numerical methods", *Math. Method. Appl. Sci.*, **47**(12), 10400-10420. https://doi.org/10.1002/mma.10129.

Yaylacı, M., Yazıcıoğlu, A., Uzun Yaylacı, E., Terzi, M. and Birinci, A. (2025), "Evaluation of the contact problem of two layers one of functionally graded, loaded by circular rigid block and resting on a Pasternak foundation by analytical and numerical (FEM and MLP) methods", *Arch. Appl. Mech.*, **95**(4), 1-23. https://doi.org/10.1007/s00419-025-02787-7.

Yazdani, H. and Ashtiani, M. (2023), "The behaviour of a strip footing resting on geosynthetics-reinforced slopes", *Geomech.*

Eng., **34**(6), 623-636. https://doi.org/10.12989/gae.2023.34.6.623.

CC